CFD Study of Cavity Flows

D. Lawrie, P. Nayyar

K. Badcock, G. Barakos and B. Richards

CFD Laboratory

Department Of Aerospace Engineering

University of Glasgow

Glasgow G12 8QQ

UK

www.aero.gla.ac.uk/Research/CFD

Abstract

Modern high performance military aircraft are designed for stealthy operation. This design approach dictates that stores are to carried inside protected cavities on the aircraft's fuselage. However, during certain phases of operation the aircraft will have to fly with the cavities exposed to the free-stream. During this phase an unsteady, highly energetic flow field develops inside the cavity causing structural, acoustic and aerodynamic problems. The seminal work of Rossiter and Kurn at RAE [1] provided a first understanding of the phenomena associated with cavity flow and was adequate for alleviating most of the problems encountered in the aircraft of the late 1960s and early 1970s. Recent designs, however, must deal with light weight materials and smart stores, requiring that the effect of the intense levels of sound be known. This is to ensure structural integrity and prevent damage to the sensitive electronic components integrated in modern weapons. Also modern aircraft have additional requirements for quieter and stealthier operation. For these reasons aerospace engineers are now revisiting the cavity flow problem attempting to develop a better understanding of this complex flow and improve their design methodologies.

The geometry under investigation is a simple rectangular open cavity whose length-to-depth ratio (l/d) is 5. For the high Reynolds number cases the Mach and Reynolds numbers set to 0.85 and 6.783 million, respectively. For the low Reynolds cases the Reynolds number was set to 37000 where the Mach number was varied between 0.3 and 0.9.

Several cavity flow computations were performed using PMB [2] (Parallel Multi-Block), the in-house URANS solver of the University of Glasgow in conjunction with several different turbulence models. Results demonstrated

a strong sensitivity of the flow to the emplloyed turbulence model. Of the two turbulence models employed it has been found that the SST baseline model provides consistent results compared with the k-ω model. It has also been identified that low Reynolds number cases exhibit two main flow configurations, namely a wake mode and a shear-layer mode. For high Reynolds numbers only the shear-layer mode has been identified.

Nomenclature

CFD	Computational Fluid Dynamics
d	Cavity depth
DES	Detached Eddy Simulation
l	Cavity length
LES	Large Eddy Simulation
M	Mach number
MUSCL	Monotone Upstream Centered Schemes for Conservation Laws
N	New vortex
P	Primary vortex
PMB	Parallel MultiBlock - solver
P_{mean}	Mean pressure
P_{ref}	Pressure reference to audible sound, $P_{ref} = 2\text{x}10^5\text{Pa}$
P_{rms}	Root mean square pressure, $P_{rms} = \sqrt{\frac{(\sum P - P_{mean})^2}{N}}$
RAE	Royal Aircraft Establishment
RANS	Reynolds Averaged Navier Stokes
Re	Reynolds number, $R_e = \frac{\rho u l}{\mu}$
S	Secondary vortex
SPL	Sound Pressure Level, $SPL = 20log_{10}\left(\frac{Prms}{Pref}\right)$
URANS	Unsteady Reynolds Averaged Navier Stokes
y^+	Law of the wall, $y^+ = (\frac{\rho}{\mu}\frac{\delta u}{\delta y})_w^{1/2} y$

Introduction

Cavity flows have been the subject of much study over the last 60 years. During the fifties a great deal of literature was produced on the cavity flow problem. Most of this work focussed on the acoustics and unsteadiness inherent in the problem. Interest in cavity flows has resurfaced again due to the need for the internal carriage of weapons stores in order to reduce the drag and radar profile of modern aircraft (Figure 1). Nevertheless, undesirable features are associated with cavities. These include aircraft volume requirements and constraints on store geometry and size. In addition, for long cavities, it has been observed that undesirable pitching moments may be generated on the stores, causing them to return and strike the aircraft that released them.

These problems effect the stores and internal equipment of the aircraft and as such they have to be qualified to the most severe sound pressure levels anticipated for a given mission. This requires for the cavity acoustics to be understood and for tools to be developed allowing reliable predictions of cavity flow aerodynamics.

As of today, a significant amount of research has been carried out on cavity flows both experimentally [3,4] and computationally [5,6]. Experiments which Rossiter [1] performed in water tanks, allowed the first simple calculation of the cavity frequencies to be performed. However, the amplitudes of each of these frequencies still cannot be derived from his analysis. It remains to be seen whether CFD tools will allow for predictions of both frequencies

and amplitudes along with providing information on the flow structures inside and around the cavities.

Apart from providing basic understanding of cavity flows, research has also been undertaken on cavity configurations closer to the actual weapons bays found on aircraft. Ross *et al.* [4] performed extensive experimental tests on a cavity at various freestream conditions and examined the effects of having the cavity doors present at various angles of opening. This work has provided the experimental data used in the present study for the high Reynolds numbers.

Computational results at low Reynolds numbers have shown that there are two dominant flow patterns. The first one is termed the shear layer mode (Figure 2(a)) and its main characteristic is the vibration of the shear layer formed between the upstream and downstream ends of the cavity. The second pattern has been termed the wake mode [5] (Figure 2(b)) and is dominated by vortex shedding from the downstream end of the cavity.

In this work, examination of such flows has been performed and results are included, the purpose of the investigation was to examine the transition, if any, between the shear layer and wake mode over a range of regimes.

Most of the present work was carried out in 2D. Even so the flow fields have been found to be complicated and can be difficult to predict accurately.

Numerical Method

The PMB solver [2] has been used. This code has been developed at the University of Glasgow over a number of years and has been used successfully in a variety of problems including cavity flows [6], hypersonic film cooling, spiked bodies, flutter and delta wing flows amongst others.

PMB solves the unsteady Reynolds Averaged Navier Stokes Equations on multiblock structured grids, in serial or parallel mode. Governing equations are discretised using a cell-centered finite volume method. The convective terms are discretised using Osher's upwind scheme while Roe's scheme is also available. MUSCL interpolation is used to provide nominally third order accuracy and the Van Albada limiter is used to avoid spurious oscillations across shocks. The time-marching of the solution is based on an implicit, dual time stepping method. The final algebraic system of equations is solved using a Conjugate Gradient method, in conjunction with Block Incomplete Lower Upper factorisation. A number of turbulence models have been implemented and tested including one and two-equation statistical models as well as DES and LES.

Results and Discussion

Low Reynolds number

Based on previous work [5,10] on low Reynolds number flows, a study of the cavity flow has been performed. This study examines the effects of Reynolds number and Mach number on the transition between the wake mode and the shear layer mode. A computational grid

of approximately 35000 points is used. This grid was found to give spatial convergence. The wake mode is shown to be quite different from the shear layer mode with the main difference being the collapse of the shear layer between the upstream and downstream cavity walls (Figure 2(a)) and the development of a more energetic vortical flow (Figure 2(b)) inside the cavity and continuous shedding of vorticity downstream. Results are presented for Reynolds number 37000 and Mach numbers ranging from 0.3 to 0.9.

In Figure 3, results for the pressure field inside a cavity of l/d=5 at Re=37000 are presented. It can be seen that at the leading edge of the cavity a large vortical structure is formed, this vortex continues to feed off the separated flow at the leading edge and grows to a size approximately equal to the cavity depth. At the same time there is a build up of negative vorticity along the wall, relative to the primary vortex [P]. This rolls up into a secondary vortex [S] which causes the large primary vortex to finally separate from the leading edge (Figure 3(b)). This massive separation also causes the laminar boundary layer upstream of the leading edge to separate, resulting in a new vortex which will replace the primary vortex now convecting downstream. As the primary vortex is convected downstream a new vortex [N] 'drops' into the cavity and begins to grow in size fed by the separated flow at the leading edge (Figure 3(c)). The primary vortex at this point will impact against the rear wall and split. Part of the vortex will convect downstream and the remaining will eventually be absorbed by a new vortex as it is shed off the leading edge. It is noted that the secondary vortex, once rid of the primary vortex which created it dissipates very quickly (Figures 3(c) and 3(d)).

On lowering the Mach number (Figure 4) it was observed that there appears to be blending between the two modes, indicating a gradual transition rather than a switch from one mode to the other. In Figure 4(a) it can be seen that the primary and secondary vortices are both present as in the Mach 0.6 case (Figure 3(a)). This indicates that the wake mode is present, however as the cycle continues, the mechanism is also slightly altered due to the presence of the shear layer mode. Figure 4(b) shows the vortex convected downstream such that it is about to impact on the rear wall. It can be seen from this that the size of the primary vortex is again larger than the cavity depth but smaller than for the pure wake mode case (Figure 3(c)). As the cycle progresses, additional vortices are produced and appear to merge together to create the large primary vortex (Figures 4(c) and 4(d)). At the low Mach number end of the scale, the blending causes the shear layer to fully span the cavity (Figure 4(b)). It s to be noted, however, that unlike the two vortex system in high Reynolds numbers, in which turbulence becomes a factor, there are many vortices in the cavity. This is due to the viscous effects being reduced at these Reynolds numbers and thus the vortices can form more easily. At even lower Mach numbers the size of the primary vortex is expected to shrink further and produce a cavity cycle similar to the shear layer mode.

At higher Mach numbers (Figure 5) a blending similar to the Mach 0.4 case can be seen. The nature of the blending appears to be Mach dependent as the blending at low Mach numbers is slightly different to the higher Mach numbers examined so far. In Figure 5(a) it can be seen that instead of a single primary vortex two adjacent vortices appear. These vortices will merge together to form the primary vortex (Figure 5(b)) and this will be convected downstream as in the pure wake mode case. Thus the cycle is shown to mainly progress as for the wake mode (Figures 5(c) and 5(d)) but also to be moving towards the two vortex cycle seen in the shear layer mode case. At higher Mach numbers the shear layer mode is expected to become more and more dominant.

High Reynolds number

As reported by previous authors[6], CFD results for cavities of l/d=5 at Re=6.783x10^6 and M=0.85 were sensitive to the refinement of the computational grid. The present work attempts to shed some light on this problem. The cavity cycle for the turbulent cases is somewhat different than the low Reynolds number cases. In the high Reynolds number regime the vortex shedding previously seen (Figure 3) does not occur, instead a system of vortex stretching, splitting and convecting occurs coupled with shear layer displacement and acoustic radiation. As shown in Figure 6 two vortices exist in the cavity. It should be noted that the shear layer spans the whole length of the cavity, thus it is of the open class of cavity according to the designation found in [3]. In this case, the secondary vortex [S] continues to grow in size and stretches to fill the cavity (Figure 6), the primary vortex [P] continues to lose strength due to mass expulsion at the cavity wall. The secondary vortex eventually becomes the only vortex in the cavity. At this point, the vortex has stretched most of the way along the cavity but has been unable to grow in any direction other than through the length of the cavity due to the shear layer constraining it. The vortex at this point splits into two new vortices. The larger downstream vortex begins to convect towards the rear wall and will replace the initial primary vortex and the smaller vortex begins to feed off the shear layer and will replace the initial secondary vortex.

During this cycle the shear layer is deflected due to the presence and interactions between the vortices and the mass ingestion and expulsion occurring at the rear wall causes the shear layer to separate and reattach. This movement of the shear layer and its impact on the wall gives rise to acoustic waves which propagate outwards and upstream.

The analysis presented above is based on the results using the k-ω model. Additional results are also obtained using the SST model, as it showed a quite different response during spatial and temporal refinements.

For the temporal refinement the coarse grid was used. The employed time step, and hence the frequency range that could be captured, was altered such that for the coarse time case the time step was 0.01 and the fine time step was 0.001 dimensionless units.

The effect the spatial refinement had on the

k-ω model was unexpected (Figure 7(a)), it caused a shift in the dominant Rossiter mode to a lower frequency. This can be seen by the change in the shape of the SPL plot which is a statistical measure of the intensity of the acoustics with reference to the audible sound range. The shape of the SPL curves is created by the various frequencies, the more dominant the frequency the more pronounced the shape of the corresponding mode in the overall sound pressure levels. In the case of the l/d ratio case examined here the second mode (approximately 380Hz), corresponding to the 'w' shape, should be dominant. It was found that the first mode (approximately 160Hz), corresponding to the 'v' shape, became dominant.

After some investigation the reason for this shift in the dominant mode was found. The method used to refine the grid spatially was found to be the cause. In this case the y^+ value was being adversely affected. The effect of reducing the y^+ value is that the turbulent specific dissipation rate increases, this corresponds to a drop in the turbulent kinetic energy. When the same refinement method was used on the SST model, to examine the dependency on wall functions, the effect was found to be different. For the SST model the effect of this refinement method was found to increase the amplitude of the frequencies (Figure 10(a)) without adversely effecting the frequencies themselves.

A temporal refinement case on the original, unrefined grid, was also examined to highlight the dependency on the base time step. For the k-ω model the temporal refinement had very little effect(Figure 7(b)) and so the grid was concluded to be refined sufficiently with the base time step. Examination of the instantaneous pressure plots plus streamlines for this case shows that the three flows, despite having different frequencies look similar(Figures 6,8(a) and 8(b)). The effect of the temporal refinement on the SST model was surprisingly similar to the effect of the spatial refinement. The only real difference was to shift the amplitudes and hence further overpredict the experimental data (Figure 10(b)). It can also be seen from the instantaneous flow visualisations that the results for all three cases are in excellent agreement (Figure 9,11(a) and 11(b))

Conclusions

The PMB solver has been successfully applied to different aspects of the cavity flow problem. For the low Reynolds number cases the flow cycle has been investigated and although no experimental data is available for validation, grid and time refinement studies were used to improve our confidence in the obtained results. It has been demonstrated that the method of transition between the wake and shear layer mode appears to be a gradual transition, with the flow taking on aspects of both modes.

The wake mode was found to be dominant at low Reynolds cases with the shear layer mode appearing towards high Mach and high Reynolds numbers.

With regards to the high Reynolds number results it has been seen that the k-ω model was able to produce results in good agreement with experiments. It failed, however, to provide grid converged solutions. The SST model, in contrast, has been shown to produce different re-

sults, this model appears to be quite robust and gives consistent predictions for the overall SPL of cavity flows.

At present calculations, both for the low and high Reynolds number regimes are being undertaken in 3D. These cases will now be further extended to include door at various angles and the inclusion of stores into the cavity to effect a fuller understanding of these flows in practical situations.

Acknowledgements

The financial support by QinetiQ Ltd. and BAE SYSTEMS is gratefully acknowledged.

References

1. J.E. Rossiter and A.G. Kurn, Wind tunnel measurements of the unsteady pressures in and behind a bomb bay (Canberra), RAE Tech. Note Aero 2845, October 1963.

2. K. Badcock, F. Cantariti and B. Gribben, Theory Guide to Pmb2D Version 3.1, Aerospace Engineering Department Report University of Glasgow, June 2000.

3. M.B. Tracey and E.B. Plentovich, Characterization Of Cavity Flow Fields Using Pressure Data Obtained in the Langley 0.3-Meter Transonic Cryogenic Tunnel, NASA Technical Report 4436, March 1993.

4. J.A. Ross and J.W. Peto, The Unsteady Environment within an Internal Weapons Bay or Cavity, DERA Report, November 1992.

5. T. Colonius and A.J. Basu and C. Rowley, Numerical Investigation of the Flow Past a Cavity, AIAA/CEAS 5th Aeroacoustics Conference 99-1912, May 1999.

6. J. Henderson, Investigation of Cavity Flow Aerodynamics using Computational Fluid Dynamics, *PhD Thesis, Department of Aerospace Engineering*, University Of Glasgow, August 2001.

7. D. P. Rizzetta, Numerical Simulation of Supersonic Flow over a Three- Dimensional Cavity, AIAA Journal Vol.36 No.7, July 1988.

8. N.E. Suhs and A. AFS, Computations of Three-Dimensional Cavity Flow at Subsonic and Supersonic Mach Numbers, 19th AIAA Fluid Dynamics, Plasma Dynamics and Lasers Conference, 87-1208, June 1987.

9. N. Taborda, D. Bray and K. Knowles Visualisation of Three Dimensional, Transonic Cavity Flows, 5th World Conference on Experimental Heat Transfer, Fluid Mechanics and Thermodynamics, September 2001.

10. M. Shieh, Parallel Numerical Simulations of Subsonic, Turbulent, Flow Induced Noise from Two- and Three-Dimensional Cavities Using Computational Aeroacoustics, *PhD Thesis, Pennsylvania State University Department Of Aerospace Engineering*, May 2000.

11. F.R. Menter, Two-Equation Eddy-Viscosity Turbulence Models for Engineering Applications, AIAA Journal Vol.32 No.8, August 1994.

Figure 1: Bomb bay of a B17.

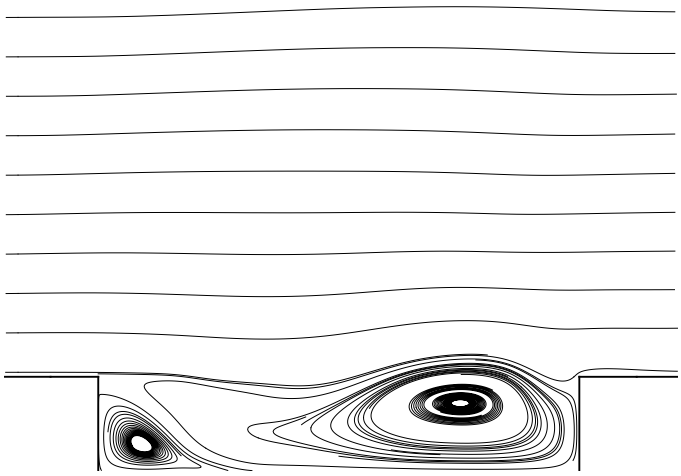

(a) Schematic of the shear layer mode.

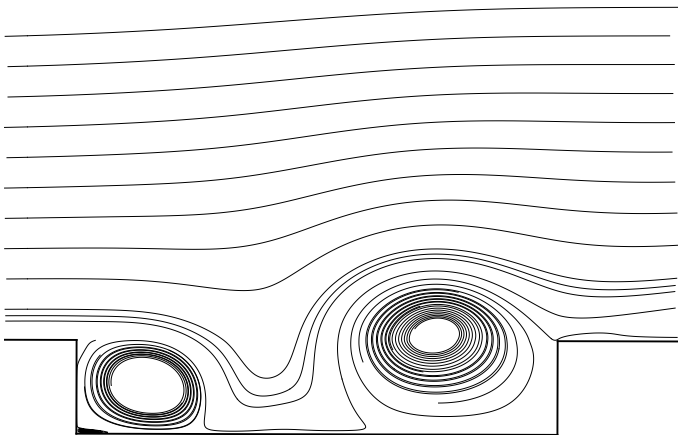

(b) Schematic of the wake mode.

Figure 2: Comparison of cavity flow modes.

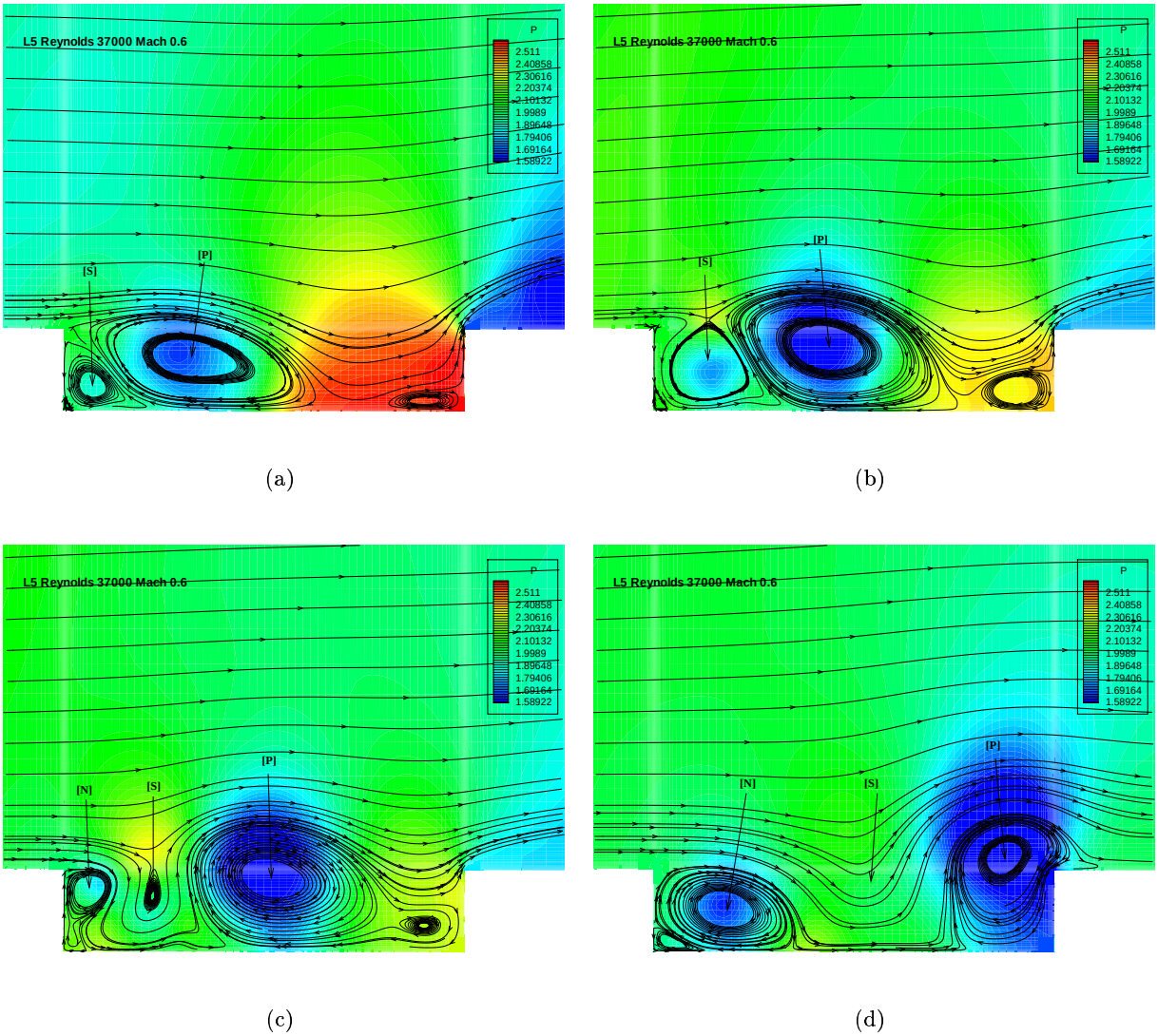

(a) (b)

(c) (d)

Figure 3: Pressure contours and super-imposed instantaneous streamlines for the Mach 0.6 case exhibiting the wake flow mode (Re=37000, l/d=5, dt=0.1).

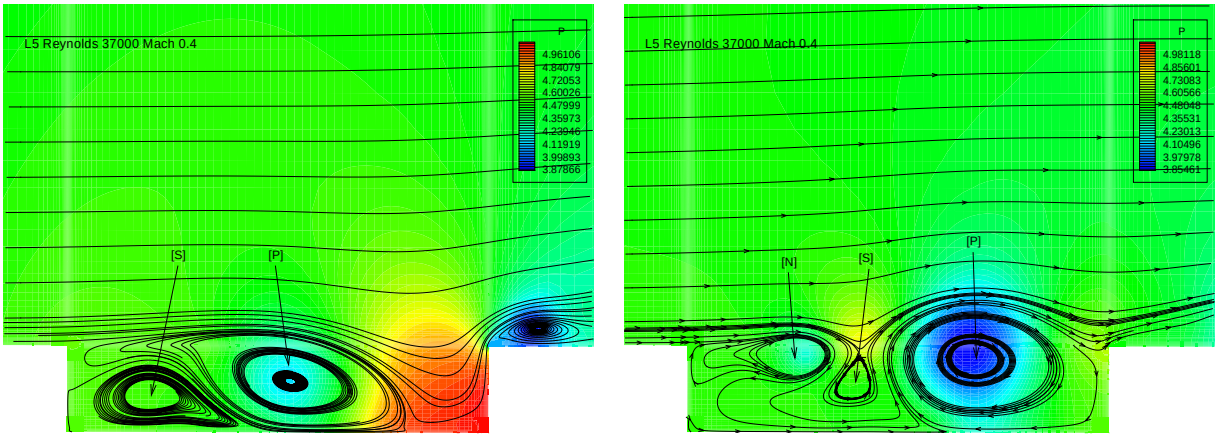

(a) (b)

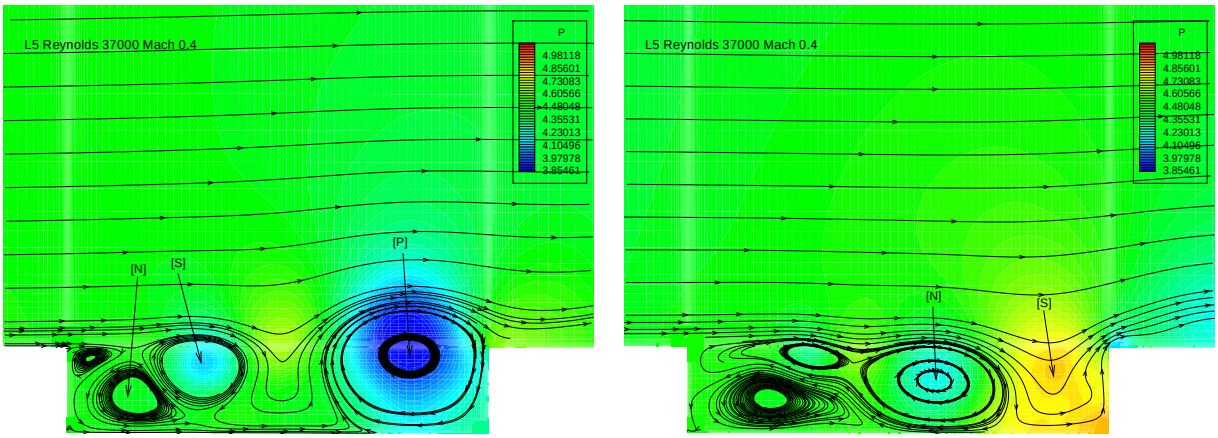

(c) (d)

Figure 4: Pressure contours and super-imposed instantaneous streamlines for the Mach 0.4 case exhibiting wake mode like flow (Re=37000, l/d=5, dt=0.1).

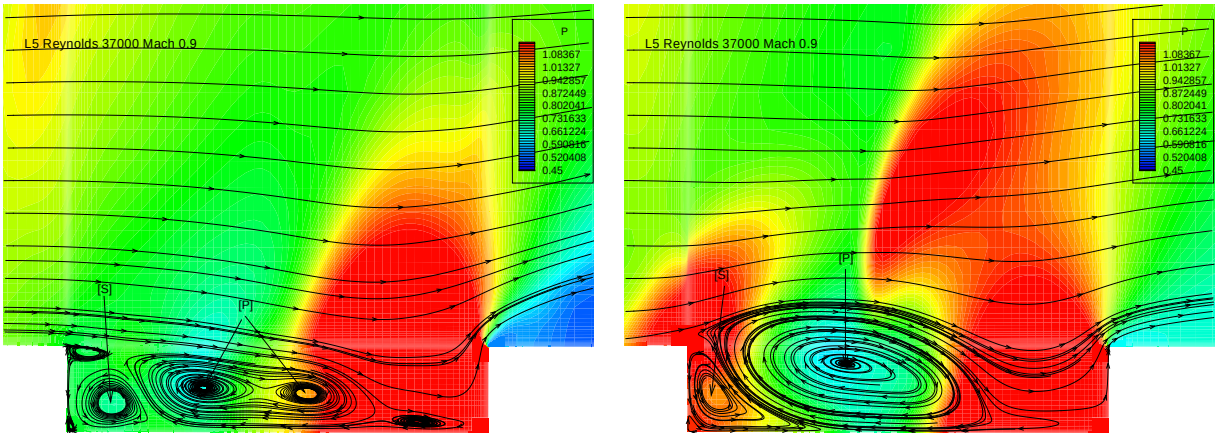

(a) (b)

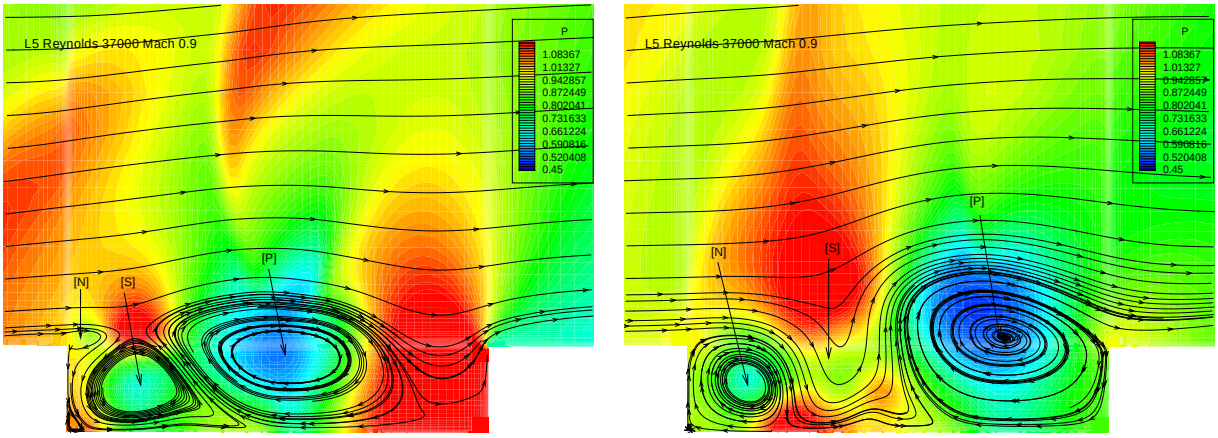

(c) (d)

Figure 5: Pressure contours and super-imposed instantaneous streamlines for the Mach 0.9 case exhibiting wake mode like flow (Re=37000, l/d=5, dt=0.1).

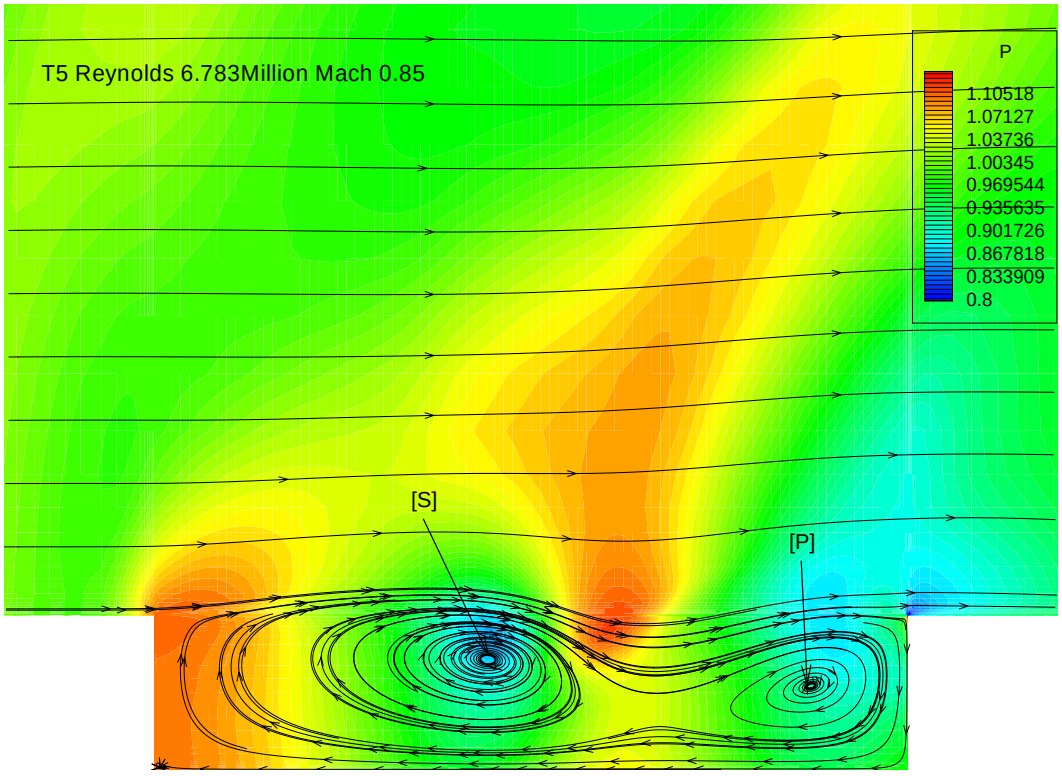

Figure 6: T5 k-ω model base grid

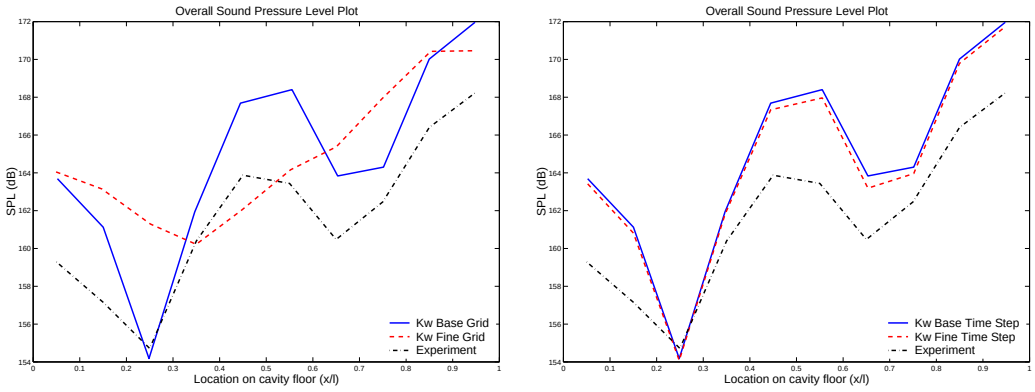

(a) k-ω model base vs. spatial fine grid SPL

(b) k-ω model base vs. time fine grid SPL

Figure 7: SPL plots predicted using the k-ω model. These plots were constructed using 10 pressure points in the calculation. All SPL points correspond to the pressure taps used by Ross *et al.* [4] in the experiment.

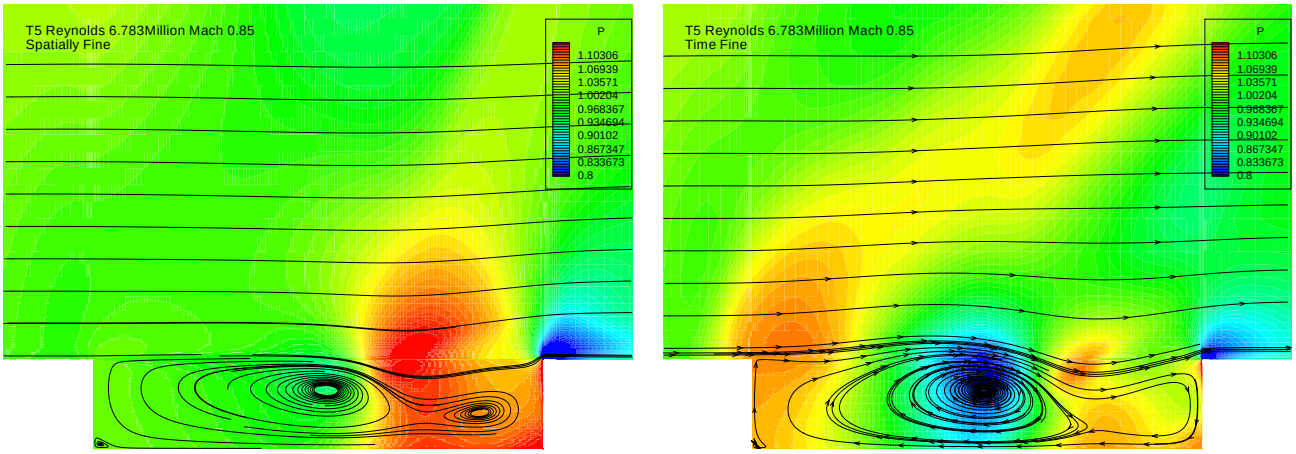

(a) k-ω model fine grid - spatial refinement

(b) k-ω model fine grid - temporal refinement

Figure 8: Visualisation of the results of the flow using the k-ω model - effect of spatial and temporal refinement.

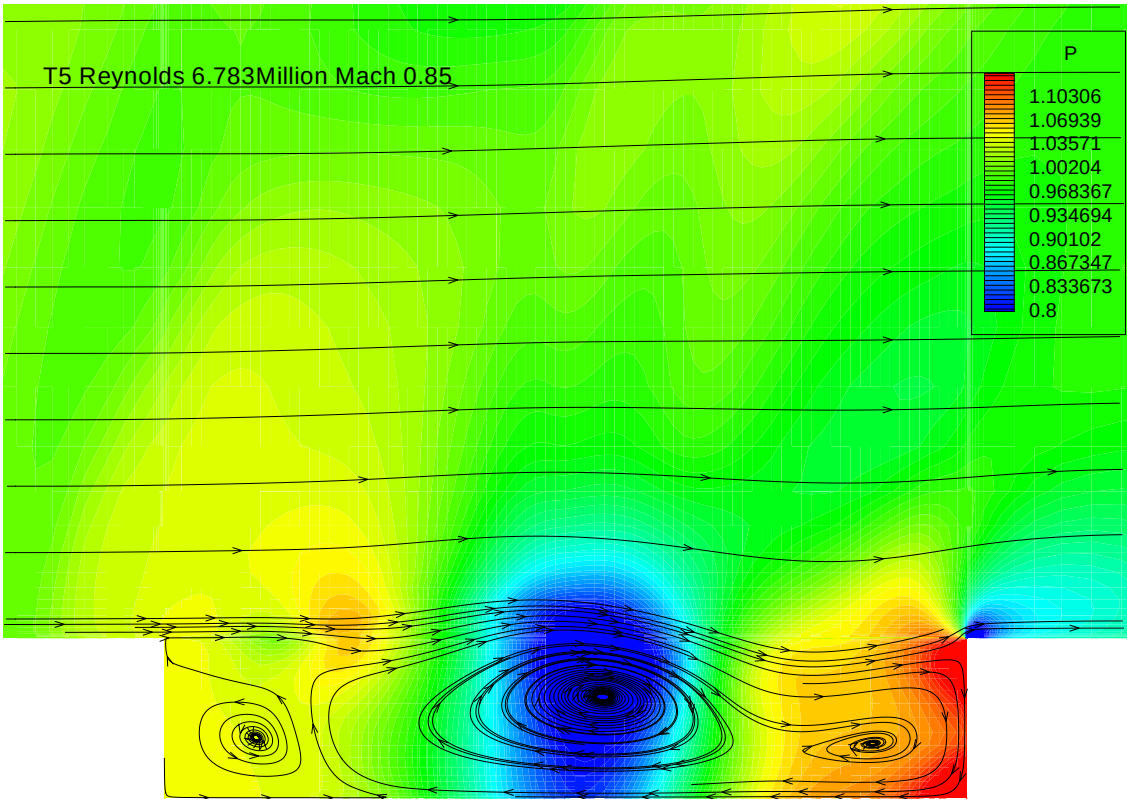

Figure 9: T5 SST model base grid.

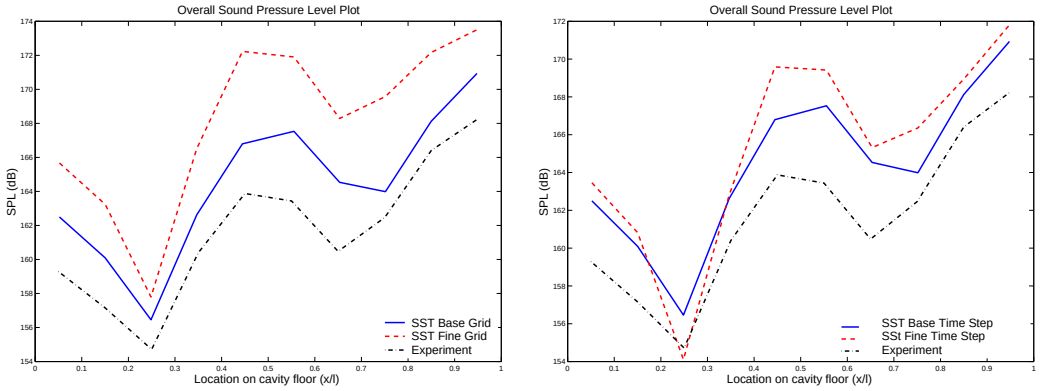

(a) SST model base vs. spatial fine grid SPL

(b) SST model base vs. time fine grid SPL

Figure 10: SPL plots predicted using the SST model. These plots were constructed using 10 pressure points in the calculation. All SPL points correspond to the pressure taps used by Ross *et al.* [4] in the experiment.

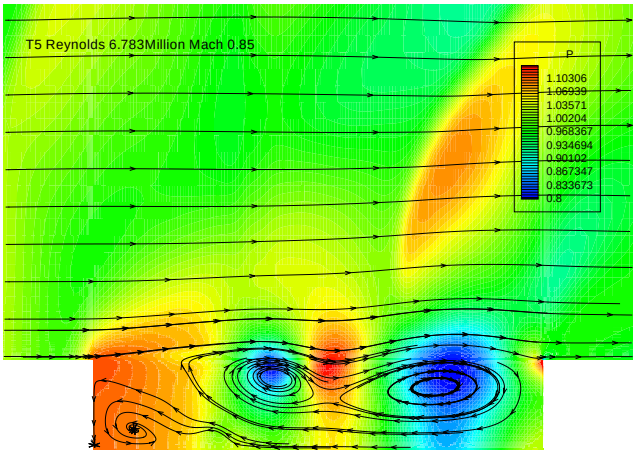

(a) SST model fine grid - spatial refinement

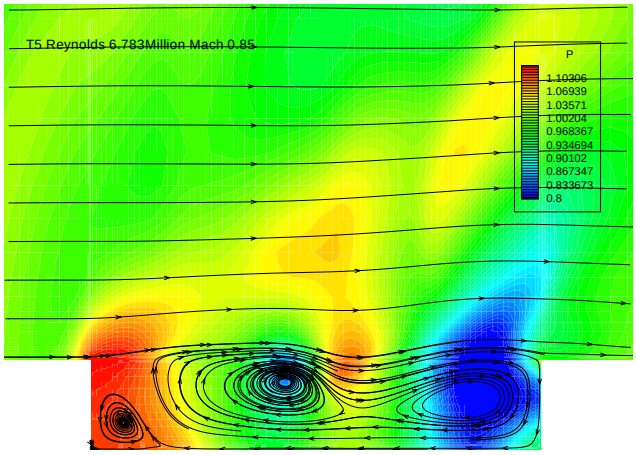

(b) SST model fine grid - temporal refinement

Figure 11: Visualisation of the results of the flow using the SST model - effect of spatial and temporal refinement.